Computers and Concrete, *Vol. 19, No. 3 (2017) 325-331*
DOI: https://doi.org/10.12989/cac.2017.19.3.325

Mathematical modeling of concrete pipes reinforced with CNTs conveying fluid for vibration and stability analyses

Alireza Zamani Nouri*

Department of Civil Engineering, college of Engineering, Saveh Branch, Islamic Azad University, Saveh, Iran

(Received November 29, 2016, Revised January 7, 2016, Accepted January 10, 2016)

Abstract. In this study, vibration and stability of concrete pipes reinforced with carbon nanotubes (CNTs) conveying fluid are presented. Due to the existence of CNTs, the structure is subjected to magnetic field. The radial fore induced with fluid is calculated using Navier-Stokes equations. Characteristics of the equivalent composite are determined using Mori-Tanaka model. The concrete pipe is simulated with classical cylindrical shell model. Employing energy method and Hamilton's principal, the motion equations are derived. Frequency and critical fluid velocity of structure are obtained analytically based on Navier method for simply supported boundary conditions at both ends of the pipe. The effects of fluid, volume percent of CNTs, magnetic field and geometrical parameters are shown on the frequency and critical fluid velocity of system. Results show that with increasing volume percent of CNTs, the frequency and critical fluid velocity of concrete pipe are increased.

Keywords: concrete pipe; fluid; modeling; critical fluid velocity; vibration

1. Introduction

Concrete pipeline systems have been the material of choice for over a century and remain the most environmentally friendly and competitive installed option today. Compared to other pipeline materials, concrete provides a wide range of alternative bedding designs which can lead to substantial installed cost savings, faster installation and lower environmental impact. A proven service life of 100 years ensures that lifetime costs are kept to a minimum. The inherent strength and durability of precast concrete can help protect the system throughout its operation, during maintenance and extend replacement periods. Nowadays, applying the nanotechnology to produce the concrete structures has been a new field in experimental and theoretical works. Hence, in this paper, the concrete pipe is simulated with cylindrical shell model to investigate the effect of CNTs as reinforce of this structures.

The study of vibration behavior of circular cylindrical shells has therefore been carried out extensively by many investigators. Junger and Mass (1952), and later Jain (1974) studied coupled vibrations of fluid-filled cylindrical shells based on shear shell theory and discussed the free vibration of orthotropic cylindrical shells filled partially or completely with an incompressible, non-viscous fluid. Frequency response of cylindrical shells partially submerged or filled with liquid was investigated by Goncalves and Batista (1987). An exact solution to the free vibration of a transversely isotropic cylindrical shell filled with fluid was proposed by Chen and Ding (199). Chung (1981) compared analytical and experimental investigations carried out by him on the vibration characteristics of cylindrical shells filled with fluid. Amabili (1996) obtained natural frequencies and mode shapes of a simply-supported circular cylindrical shell, partially filled with liquid and further extended his study to include the free vibrations of these shells entirely filled with a dense fluid and partially immersed in various fluids under different end conditions (Amabili (1999)). Pellicano and Amabili (2003) studied the stability and vibration of empty and fluid-filled circular cylindrical shells under static and periodic axial loads. Chen *et al.* (2004) improved the previous work by introducing three-dimensional vibration analysis of fluid-filled orthotropic functionally graded piezoelectric cylindrical shells. Later, free vibrations of fluid-filled cylindrical shells embedded in an elastic foundation was investigated by Gunawan *et al.* (2005) who studied the effects of fluid and elastic foundation parameters such as spring stiffness on the natural frequency of the shell. Recently, Daneshmand and Ghavanloo (2010) investigated the coupled free vibration analysis of a fluid-filled rectangular container with a sagged bottom membrane. Also, coupled vibration of a partially fluid-filled cylindrical shell was studied by Askari *et al.* (2011) who considered the effect of free surface waves in their analysis. A new calculation method was developed by Zhu *et al.* (2013) based on these properties and an explicit iterative algorithm. Using a mesoscopic finite-element (FE) mesh, three-phase composites of concrete namely aggregate, mortar matrix and interfacial transition zone (ITZ) were modelled b Zhang *et al.* (2015).

It is worth noting that none of the articles mentioned above considered nano-composite structures. Vibration analysis of SCCS with great potentials in manufacturing of actuators and sensors slows the transmission of gases and moisture vapor as a consequence of their exceedingly high surface area-to-volume ratio. Regarding composites, Gibson

*Corresponding author, Ph.D.
E-mail: Dr.zamani.ar@gmail.com

ISSN: 1598-8198 (Print), 1598-818X (Online)

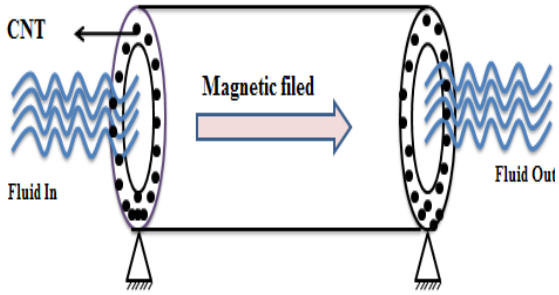

Fig. 1 A concrete pipe modeled with cylindrical shell conveying fluid

and Ronald (1994) studied numerical behavior of composite materials when subjected to mechanical and thermal loading. The embedding of piezoelectric materials in the form of fibers into a polymer matrix was implemented by Bent *et al.* (1995). Free vibration of composite plates and cylindrical shell panels were studied by Messina and Soldatos (1999) using a higher-order theory. Micro-electro-mechanical models were afterwards used by Tan and Tong (2001) to predict the equivalent characteristics for piezoelectric-fiber-reinforced composite materials. They investigated effects of geometrical parameters on the effective electroelastic constants, and discussed the convergence of the rectangle-cylinder model. Free vibration and buckling analysis of composite cylindrical shells conveying hot fluid were proposed by Kadoli and Ganesan (2003). Active control of laminated cylindrical shells using piezoelectric fiber reinforced composites was investigated by Ray and Reddy (2005). In another study, vibration and buckling of cross-ply laminated composite circular cylindrical shells were studied by Matsuna (2007) based on a global higher-order theory. Rahmani *et al.* (2010) investigated free vibration response of composite sandwich cylindrical shells with flexible core. Buckling and vibration analysis of plate/shell structures via a smoothed quadrilateral flat shell element with in-plane rotations were studied by Nguyen-Van (2011). Zamanian *et al.* (2016). the nonlinear buckling of straight concrete columns armed with single-walled carbon nanotubes (SWCNTs) resting on foundation was investigated by Safari Bilouei *et al.* (2016). Stress analysis of concrete pipes reinforced with AL2O3 nanoparticles was presented by Heidarzadeh *et al.* (2016) considering agglomeration effects.

So far, very few researchers have used mathematical modeling for concrete structures. Presenting a mathematical modeling in this study, vibration and stability of concrete pipes reinforced with CNTs conveying fluid are investigated. The structure is subjected to magnetic field and simulated with classical cylindrical shell model. Based on analytical method, the frequency and critical fluid velocity of pipe are obtained. The effects of the fluid, volume percent of CNTs, magnetic field and geometrical parameters on the frequency and critical fluid velocity of the structure are investigated.

2. Mori-Tanaka model

Consider a pipe whose shell is concrete, and is reinforced by CNTs which is shown in Fig. 1. The pipe is reinforced with CNTs and conveying fluid.

Using Mori-Tanaka model (Tan *et al.* 2005), the matrix is assumed to be isotropic and elastic, with the Young's modulus E_m and the Poisson's ratio v_m. The constitutive relations for a layer of the composite with the principal axes parallel to the r, θ and z directions are

$$\begin{Bmatrix}\sigma_{11}\\ \sigma_{22}\\ \sigma_{33}\\ \sigma_{23}\\ \sigma_{13}\\ \sigma_{12}\end{Bmatrix}=\begin{bmatrix}k+m & l & k-m & 0 & 0 & 0\\ l & n & l & 0 & 0 & 0\\ k-m & l & k+m & 0 & 0 & 0\\ 0 & 0 & 0 & p & 0 & 0\\ 0 & 0 & 0 & 0 & m & 0\\ 0 & 0 & 0 & 0 & 0 & p\end{bmatrix}\begin{Bmatrix}\varepsilon_{11}\\ \varepsilon_{22}\\ \varepsilon_{33}\\ \gamma_{23}\\ \gamma_{13}\\ \gamma_{12}\end{Bmatrix} \tag{1}$$

Where σ_{ij}, ε_{ij}, γ_{ij}, k, m, n, l, p are the stress components, the strain components and the stiffness coefficients respectively. According to the Mori-Tanaka method the stiffness coefficients are given by (Tan *et al.* 2005)

$$\begin{aligned}
k &= \frac{E_m\{E_m c_m + 2k_r(1+\nu_m)[1+c_r(1-2\nu_m)]\}}{2(1+\nu_m)[E_m(1+c_r-2\nu_m)+2c_m k_r(1-\nu_m-2\nu_m^2)]}\\
l &= \frac{E_m\{c_m\nu_m[E_m+2k_r(1+\nu_m)]+2c_r l_r(1-\nu_m^2)]\}}{(1+\nu_m)[E_m(1+c_r-2\nu_m)+2c_m k_r(1-\nu_m-2\nu_m^2)]}\\
n &= \frac{E_m^2 c_m(1+c_r-c_m\nu_m)+2c_m c_r(k_r n_r - l_r^2)(1+\nu_m)^2(1-2\nu_m)}{(1+\nu_m)[E_m(1+c_r-2\nu_m)+2c_m k_r(1-\nu_m-2\nu_m^2)]}\\
&\quad + \frac{E_m[2c_m^2 k_r(1-\nu_m)+c_r n_r(1+c_r-2\nu_m)-4c_m l_r\nu_m]}{E_m(1+c_r-2\nu_m)+2c_m k_r(1-\nu_m-2\nu_m^2)}\\
p &= \frac{E_m[E_m c_m+2p_r(1+\nu_m)(1+c_r)]}{2(1+\nu_m)[E_m(1+c_r)+2c_m p_r(1+\nu_m)]}\\
m &= \frac{E_m[E_m c_m+2m_r(1+\nu_m)(3+c_r-4\nu_m)]}{2(1+\nu_m)\{E_m[c_m+4c_r(1-\nu_m)]+2c_m m_r(3-\nu_m-4\nu_m^2)\}}
\end{aligned} \tag{2}$$

Where the subscripts m and r stand for matrix and reinforcement respectively. C_m and C_r are the volume fractions of the matrix and the nanoparticles respectively and k_r, l_r, n_r, p_r, m_r are the Hills elastic modulus for the nanoparticles (Tan *et al.* 2005).

3. Stress-strain relations

Shear strains y_{xz}, $y_{\theta z}$ are considered negligible in the Kirchhoff deformation theory. Hence, the tangential displacements u, v become linear function of the radial coordinate (z) (Ghorbanpour *et al.* 2012). In other words

$$\begin{aligned}
v(x,\theta,z) &= v(x,\theta) - z\frac{\partial w(x,\theta)}{R\partial\theta},\\
u(x,\theta,z) &= u(x,\theta) - z\frac{\partial w(x,\theta)}{\partial x},\\
w(x,\theta,z) &= w(x,\theta).
\end{aligned} \tag{3}$$

The strain components $\bar{\varepsilon}_{xx}$, $\bar{\varepsilon}_{\theta\theta}$ and $\bar{\gamma}_{x\theta}$ at an arbitrary point of the shell are related to the middle surface strains ε_{xx}, $\varepsilon_{\theta\theta}$ and $\gamma_{x\theta}$, and to the changes in the curvature

and torsion of the middle surface k_{xx}, $k_{\theta\theta}$ and $k_{x\theta}$ by the following relationships

$$\begin{Bmatrix}\varepsilon_{xx}\\ \varepsilon_{\theta\theta}\\ \varepsilon_{x\theta}\end{Bmatrix}=\begin{Bmatrix}\varepsilon_{xx}\\ \varepsilon_{\theta\theta}\\ \gamma_{x\theta}\end{Bmatrix}-z\begin{Bmatrix}k_{xx}\\ k_{\theta\theta}\\ k_{x\theta}\end{Bmatrix}=\left(\begin{bmatrix}\frac{\partial}{\partial x} & 0 & 0\\ 0 & \frac{\partial}{R\partial\theta} & \frac{1}{R}\\ \frac{\partial}{2R\partial\theta} & \frac{\partial}{2\partial x} & 0\end{bmatrix}-z\begin{bmatrix}0 & 0 & \frac{\partial^2}{\partial x^2}\\ 0 & 0 & \frac{\partial^2}{R^2\partial\theta^2}\\ 0 & 0 & 2\frac{\partial^2 w}{R\partial x\partial\theta}\end{bmatrix}\right)\times\begin{bmatrix}u\\ v\\ w\end{bmatrix}, \tag{4}$$

Where u, v and w, describe the displacements in the orthogonal coordinate system x, θ, z, established at the middle surface of the shell.

4. Motion equations

In this section, energy method and Hamilton's principal are used. The potential energy of concrete pipe is

$$U=\int_V\left(\sigma_{xx}\varepsilon_{xx}+\sigma_{\theta\theta}\varepsilon_{\theta\theta}+\sigma_{x\theta}\varepsilon_{x\theta}\right)dV, \tag{5}$$

Substituting the strain relations into potential energy yields

$$U=\int_{-h/2}^{h/2}\int_A\left(\sigma_{xx}\left(\frac{\partial u}{\partial x}-z\frac{\partial^2 w}{\partial x^2}\right)+\sigma_{\theta\theta}\left(\frac{\partial v}{R\partial\theta}+\frac{w}{R}-z\frac{\partial^2 w}{R^2\partial\theta^2}\right)+\sigma_{x\theta}\left(\frac{\partial u}{R\partial\theta}+\frac{\partial v}{\partial x}-2z\frac{\partial^2 w}{R\partial\theta\partial x}\right)\right)dz\,dA, \tag{6}$$

Defining the stress resultants as below

$$\begin{Bmatrix}N_x\\ N_\theta\\ N_{x\theta}\end{Bmatrix}=\int_{-h/2}^{h/2}\begin{Bmatrix}\sigma_{xx}\\ \sigma_{\theta\theta}\\ \tau_{x\theta}\end{Bmatrix}dz, \tag{7}$$

$$\begin{Bmatrix}M_x\\ M_\theta\\ M_{x\theta}\end{Bmatrix}=\int_{-h/2}^{h/2}\begin{Bmatrix}\sigma_{xx}\\ \sigma_{\theta\theta}\\ \tau_{x\theta}\end{Bmatrix}zdz, \tag{8}$$

Eq. (6) can be simplified as follows

$$U=\int_A\left(N_x\frac{\partial u}{\partial x}-M_x\frac{\partial^2 w}{\partial x^2}+N_\theta\left(\frac{\partial v}{R\partial\theta}+\frac{w}{R}\right)-M_\theta\frac{\partial^2 w}{R^2\partial\theta^2}+N_{x\theta}\left(\frac{\partial u}{R\partial\theta}+\frac{\partial v}{\partial x}\right)-2M_{x\theta}\frac{\partial^2 w}{R\partial\theta\partial x}\right)dA, \tag{9}$$

The kinetic energy of system can be written as

$$K=\frac{\rho}{2}\int_v\left(\left(\frac{\partial u}{\partial t}\right)^2+\left(\frac{\partial v}{\partial t}\right)^2+\left(\frac{\partial w}{\partial t}\right)^2\right)dV, \tag{10}$$

Substituting Eq. (3) into Eq. (10) and simplifying yields

$$K=\int\left(\frac{\rho}{2}\left(\frac{h^3}{12}\left(\left(\frac{\partial^2 u}{\partial t\partial x}\right)^2+\left(\frac{\partial^2 w}{\partial t\partial\theta}\right)^2\right)+h\left(\left(\frac{\partial u}{\partial t}\right)^2+\left(\frac{\partial v}{\partial t}\right)^2+\left(\frac{\partial w}{\partial t}\right)^2\right)\right)dA. \tag{11}$$

The work done by the magnetic field can be written as (Agrawal *et al.* 2016)

$$\mathrm{W}_m=\int_{-h/2}^{h/2}\underbrace{\eta h H_x^2\left(\frac{\partial^2 w}{\partial x^2}\right)}_{F_{magnet}}dz, \tag{12}$$

Where η and H_x are magnetic permeability and magnetic field, respectively.

The governing equation of the fluid can be described by the well-known Navier-Stokes equation as below (Baohui *et al.* 2012)

$$\rho_f\frac{d\mathbf{V}}{dt}=-\nabla\mathbf{P}+\mu\nabla^2\mathbf{V}+\mathbf{F}_{body}, \tag{13}$$

Where $V\equiv(v_z,\ v_\theta,\ v_x)$ is the flow velocity vector in cylindrical coordinate system with components in longitudinal x, circumferential θ and radial z directions. Also, P, μ and ρ_f are the pressure, the viscosity and the density of the fluid, respectively and F_{body} denotes the body forces. In Navier-Stokes equation, the total derivative operator with respect to t is

$$\frac{d}{dt}=\frac{\partial}{\partial t}+v_x\frac{\partial}{\partial x}+v_\theta\frac{\partial}{R\partial\theta}+v_z\frac{\partial}{\partial z}, \tag{14}$$

At the point of contact between the fluid and the core, the relative velocity and acceleration in the radial direction are equal. So

$$v_z=\frac{dw}{dt}, \tag{15}$$

By employing Eqs. (14) and (15) and substituting into Eq. (13), the pressure inside the pipe can be computed as

$$\frac{\partial p_z}{\partial z}=-\rho_f\left(\frac{\partial^2 w}{\partial t^2}+2v_x\frac{\partial^2 w}{\partial x\partial t}+{v_x}^2\frac{\partial^2 w}{\partial x^2}\right)+\mu\left(\frac{\partial^3 w}{\partial x^2\partial t}+\frac{\partial^3 w}{R^2\partial\theta^2\partial t}+v_x\left(\frac{\partial^3 w}{\partial x^3}+\frac{\partial^3 w}{R^2\partial\theta^2\partial x}\right)\right), \tag{16}$$

By multiplying two sides of Eq. (16) in the inside area of the pipe (A), the radial force in the pipe is calculated as below

$$F_{fluid}=A\frac{\partial p_z}{\partial z}=-\rho_f\left(\frac{\partial^2 w}{\partial t^2}+2v_x\frac{\partial^2 w}{\partial x\partial t}+{v_x}^2\frac{\partial^2 w}{\partial x^2}\right)+\mu\left(\frac{\partial^3 w}{\partial x^2\partial t}+\frac{\partial^3 w}{R^2\partial\theta^2\partial t}+v_x\left(\frac{\partial^3 w}{\partial x^3}+\frac{\partial^3 w}{R^2\partial\theta^2\partial x}\right)\right), \tag{17}$$

Finally, the external work due to the pressure of the fluid

may be obtained as follows

$$W_f = \int (F_{fluid}) w dA = \int \left(-\rho_f \left(\frac{\partial^2 w}{\partial t^2} + 2v_x \frac{\partial^2 w}{\partial x \partial t} + v_x{}^2 \frac{\partial^2 w}{\partial x^2} \right) + \mu \left(\frac{\partial^3 w}{\partial x^2 \partial t} + \frac{\partial^3 w}{R^2 \partial \theta^2 \partial t} + v_x \left(\frac{\partial^3 w}{\partial x^3} + \frac{\partial^3 w}{R^2 \partial \theta^2 \partial x} \right) \right) \right) w dA, \tag{18}$$

Finally, applying Hamilton's principal as follows

$$\delta \int_0^t (U - K - W_m - W_f) dt = 0, \tag{19}$$

The motion equations can be derived as

$$\frac{\partial N_{xx}}{\partial x} + \frac{\partial N_{x\theta}}{R \partial \theta} = \rho h \frac{\partial^2 u}{\partial t^2}, \tag{20}$$

$$\frac{\partial N_{\theta\theta}}{R \partial \theta} + \frac{\partial N_{x\theta}}{\partial x} = \rho h \frac{\partial^2 v}{\partial t^2}, \tag{21}$$

$$\frac{\partial^2 M_{xx}}{\partial x^2} + \frac{2 \partial M_{x\theta}}{R \partial x \partial \theta} + \frac{\partial^2 M_{\theta\theta}}{R^2 \partial \theta^2} - \frac{N_{\theta\theta}}{R} + N_{xx}^m \frac{\partial^2 w}{\partial x^2} + N_{\theta\theta}^m \frac{\partial^2 w}{R^2 \partial \theta^2} + N_{x\theta}^m \frac{2 \partial^2 w}{R \partial x \partial \theta} + F_{fluid} + F_{magnet} = \rho h \frac{\partial^2 w}{\partial t^2}, \tag{22}$$

Where $N_{xx}^m, N_{\theta\theta}^m, N_{x\theta}^m$ are external applied forces. Substituting Eq. (1) into Eqs. (7) and (8) yields

$$N_x = h \left(C_{11} \frac{\partial u}{\partial x} + C_{12} \left(\frac{\partial v}{R \partial \theta} + \frac{w}{R} \right) \right), \tag{23}$$

$$N_\theta = h \left(C_{12} \frac{\partial u}{\partial x} + C_{22} \left(\frac{\partial v}{R \partial \theta} + \frac{w}{R} \right) \right), \tag{24}$$

$$N_{x\theta} = h \left(C_{66} \left(\frac{\partial u}{R \partial \theta} + \frac{\partial v}{\partial x} \right) \right), \tag{25}$$

$$M_x = \frac{h^3}{12} \left(C_{11} \left(-\frac{\partial^2 w}{\partial x^2} \right) + C_{12} \left(-\frac{\partial^2 w}{R^2 \partial \theta^2} \right) \right), \tag{26}$$

$$M_\theta = \frac{h^3}{12} \left(C_{12} \left(-\frac{\partial^2 w}{\partial x^2} \right) + C_{22} \left(-\frac{\partial^2 w}{R^2 \partial \theta^2} \right) \right), \tag{27}$$

$$M_{x\theta} = \frac{h^3}{12} C_{66} \left(-2 \frac{\partial^2 w}{R \ \partial \theta \partial x} \right), \tag{28}$$

Substituting Eqs. (23)-(28) into Eqs. (20)-(22) yields

$$hC_{11} \frac{\partial^2 u}{\partial x^2} + \frac{hC_{12}}{R} \left(\frac{\partial^2 v}{\partial x \partial \theta} + \frac{\partial w}{\partial x} \right) + \frac{hC_{66}}{R} \left(\frac{\partial^2 u}{R \partial \theta^2} + \frac{\partial^2 v}{\partial x \partial \theta} \right) = \rho h \frac{\partial^2 u}{\partial t^2}, \tag{29}$$

$$\frac{hC_{12}}{R} \frac{\partial^2 u}{\partial x \partial \theta} + \frac{hC_{22}}{R^2} \left(\frac{\partial^2 v}{\partial \theta^2} + \frac{\partial w}{\partial \theta} \right) + hC_{66} \left(\frac{\partial^2 u}{R \partial x \partial \theta} + \frac{\partial^2 v}{\partial x^2} \right) = \rho h \frac{\partial^2 v}{\partial t^2}, \tag{30}$$

$$\begin{aligned} &\frac{h^3}{12} \left(-C_{11} \frac{\partial^4 w}{\partial x^4} - \frac{C_{12}}{R^2} \frac{\partial^4 w}{\partial x^2 \partial \theta^2} \right) + \frac{h^3}{12} \left(-\frac{C_{12}}{R^2} \frac{\partial^4 w}{\partial x^2 \partial \theta^2} - \frac{C_{22}}{R^4} \frac{\partial^4 w}{\partial \theta^4} \right) - - \frac{hC_{12}}{R} \frac{\partial u}{\partial x} \\ &- \left(\frac{hC_{22}}{R} \right) \left(\frac{\partial v}{\partial \theta} + \frac{w}{R} \right) - \rho_f h \left[\frac{\partial^2 w}{\partial t^2} + 2v_x \frac{\partial^2 w}{\partial x \partial t} + v_x^2 \frac{\partial^2 w}{\partial x^2} \right] \\ &- \mu_0 h \left[\frac{\partial^3 w}{\partial x^2 \partial t} + v_x \frac{\partial^3 w}{\partial x^3} + \frac{1}{R^2} \left(\frac{\partial^3 w}{\partial \theta^2 \partial t} + v_x \frac{\partial^3 w}{\partial \theta^2 \partial x} \right) \right] \\ &+ \eta h H_x^2 \left(\frac{\partial^2 w}{\partial x^2} \right) = \rho h \frac{\partial^2 w}{\partial t^2} \end{aligned} \tag{31}$$

5. Boundary conditions

The boundary conditions defined for two circular ends of the pipe are simply supported mechanical boundary conditions. The simply supported mechanical boundary condition is selected because in practice, simply supported ends could be achieved approximately by connecting the pipe to thin end plates and rings. Hence, the three displacement shapes may be written as (Reddy 2004)

$$\mathrm{d} = \begin{Bmatrix} u \\ v \\ w \end{Bmatrix} = \sum_{m=0}^{\infty} \sum_{n=0}^{\infty} \begin{Bmatrix} A_1 \cos(\frac{m\pi x}{a}) \cos(n\theta) \cos(\omega t) \\ A_2 \sin(\frac{m\pi x}{a}) \sin(n\theta) \cos(\omega t) \\ A_3 \sin(\frac{m\pi x}{a}) \cos(n\theta) \cos(\omega t) \end{Bmatrix}, \tag{32}$$

Where ω represents vibration frequency of the pipe, m and n are half axial and circumferential wave numbers, respectively. It should be noted that m is any positive number, while n is an integer, and A_i, (i=1,..,3) represent displacement amplitudes. Substituting Eq. (32) into motin equations yields

$$\begin{bmatrix} L_{11} & L_{12} & L_{13} \\ L_{21} & L_{22} & L_{23} \\ L_{31} & L_{32} & L_{33} \end{bmatrix} \begin{Bmatrix} u \\ v \\ w \end{Bmatrix} = 0, \tag{33}$$

Setting the determinate of above matrix equal to zero, the frequency and critical fluid velocity of structure can be obtained.

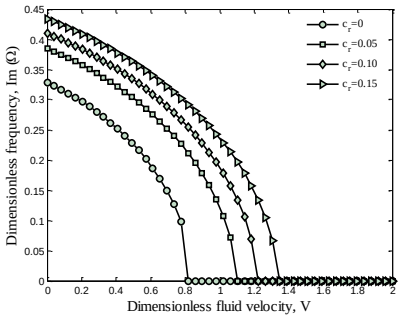

Fig. 2 The effect of CNT volume percent on the frequency of structure

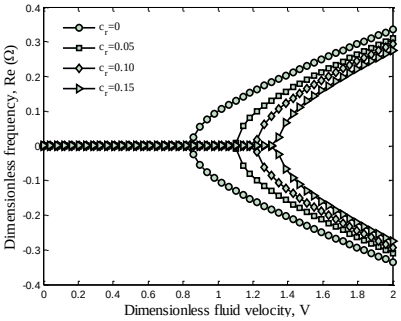

Fig. 3 The effect of CNT volume percent on the damping of structure

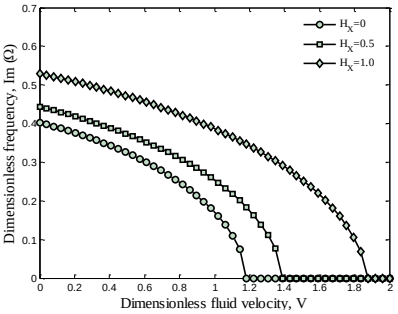

Fig. 4 The effect of magnetic field on the frequency of structure

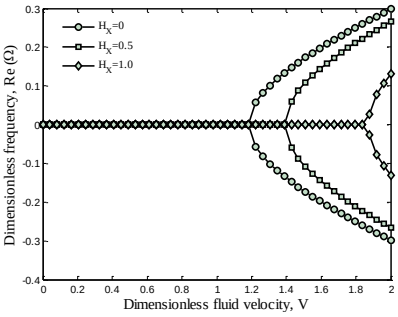

Fig. 5 The effect of magnetic field on the damping of structure

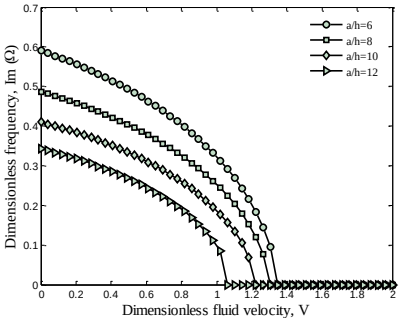

Fig. 6 The effect of length to thickness ratio on the frequency of structure

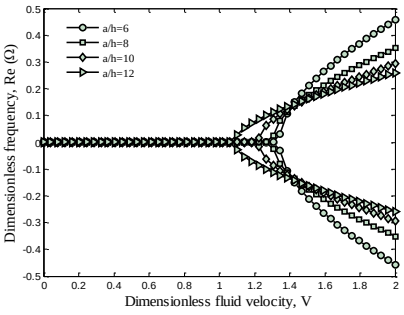

Fig. 7 The effect of length to thickness ratio on the damping of structure

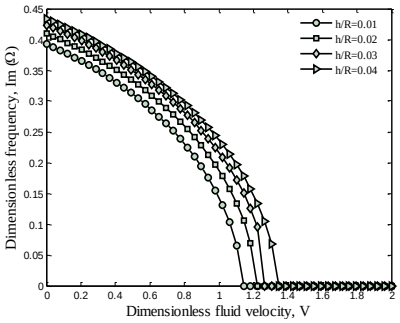

Fig. 8 The effect of thickness to radius ratio on the frequency of structure

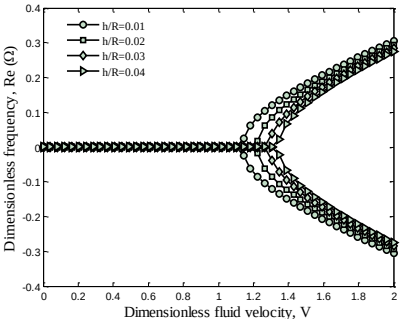

Fig. 9 The effect of thickness to radius ratio on the damping of structure

6. Result and dissection

Assuming a simply supported concrete pipe conveying water with density of ρ_f=1000 Kg/m^3, with L/h=25 and h/R=0.02. In the following subsections, the effects of fluid, volume percent of CNTs, magnetic field and geometrical parameters of pipe on the frequency and critical fluid velocity of the structure are studied and discussed in details. Figs. 2 and 3 show the CNT volume percent on the frequency (Im(Ω)) and damping (Re(Ω)) of structure ($\Omega = \sqrt{C_{11}/\rho_f}\,\omega$) versus flow velocity ($V = \sqrt{\rho_f / C_{11}}\,v_x$,) in

the dimensionless form, respectively. As can be seen, Im(Ω) decreases with increasing *V*, while the Re(Ω) remains zero.

These imply that the system is stable. When the natural frequency becomes zero, critical velocity is reached, which the system loses its stability due to the divergence via a pitchfork bifurcation. Hence, the Eigen frequencies have the positive real parts, which the system becomes unstable. In this state, both real and imaginary parts of frequency become zero at the same point. Therefore, with increasing flow velocity, system stability decreases and became susceptible to buckling. Furthermore, increasing CNT volume percent yields to increases in the Im(Ω). This is because increasing the CNT volume percent implies stiffer structure.

In realizing the influence of magnetic field, Figs. 4 and 5 show how dimensionless frequency and damping of concrete pipe changes with respect to dimensionless fluid velocity. It is found that from Fig. 4, the Im(Ω) and critical flow velocity for the structure increase with the increase of magnetic field. It is due to the fact that with increasing the magnetic field, the stiffness of structure increases.

Figs. 6 and 7 illustrate the effect of length to thickness ratio (*a/h*) on the Im(Ω) and Re(Ω) versus *V*, respectively. The results indicate that with increasing length to thickness ratio, the frequency and critical flow velocity of concrete pipe are decreased. Figs. 8 and 9 show the variation of dimensionless frequency and damping versus dimensionless fluid velocity for different thickness to radius ratio (*h/R*). It can be observed that the frequency and critical flow velocity of concrete pipe are increased with increasing thickness to radius ratio. It is because with increasing length to thickness ratio and decreasing thickness to radius ratio, the stiffness of structure is decreased.

7. Conclusions

Applying classical cylindrical shell model, the vibration and stability of a concrete pipe reinforced with CNT were investigated. The pipe was conveying fluid and the structure was subjected to magnetic field. Using an analytical method, the frequency and critical fluid velocity of structure were derived. Following investigating the volume percent of CNTs, geometrical characteristics of the structure, fluid and magnetic field, it could be said that increasing volume percent of CNTs, increased frequency and critical fluid velocity. Applying the magnetic field to the structure leads to higher frequency and critical fluid velocity. It was also concluded that with increasing length to thickness ratio and decreasing thickness to radius ratio, the frequency and critical fluid velocity of structure were decreased.

References

Agrawal, S., Gupta, V.K. and Kankar, P.K. (2016), "Static analysis of magnetic field affected double single walled carbon nanotube system", *Proc. Technol.*, **23**, 84-90.

Amabili, M. (1996), "Free vibration of partially filled horizontal cylindrical shells", *J. Sound Vibr.*, **191**(5), 757-780.

Amabili, M. (1999), "Vibrations of circular tubes and shells filled and partially immersed in dense fluids", *J. Sound Vibr.*, **221**(4), 567-585.

Askari, E., Daneshmand, F. and Amabili, M. (2011), "Coupled vibrations of a partially fluid-filled cylindrical container with an internal body including the effect of free surface waves", *J. Fluid. Struct.*, **27**(7), 1049-1067.

Baohui, L., Hangshan, G., Yongshou, L. and Zhufeng, Y. (2012), "Free vibration analysis of micropipe conveying fluid by wave method", *Res. Phys.*, **2**, 104-109.

Bent, A.A., Hagood, N.W. and Rodgers, J.P. (1995), "Anisotropic actuation with piezoelectric fiber composites", *J. Intel. Mater. Syst. Struct.*, **6**(3), 338-349.

Chen, W.Q. and Ding, H.J. (1999), "Natural frequencies of fluid-filled transversely isotropic cylindrical shells", *J. Mech. Sci.*, **41**(6), 677-684.

Chen, W.Q., Bian, Z.G. and Ding, H.J. (2004), "Three-dimensional vibration analysis of fluid-filled orthotropic FGM cylindrical shells", *J. Sol. Struct.*, **46**(1), 159-171.

Chung, H. (1981), "Free vibration analysis of circular cylindrical shells", *J. Sound Vibr.*, **74**(3), 331-359.

Daneshmand, F. and Ghavanloo, E. (2010), "Coupled free vibration analysis of a fluid-filled rectangular container with a sagged bottom membrane", *J. Fluid. Struct.*, **26**(2), 236-252.

Ghorbanpour, A.A., Kolahchi, R., Mosalaei, B.A.A. and Loghman, A. (2012), "Electro-thermo-mechanical behaviors of FGPM spheres using analytical method and ANSYS software", *Appl. Math. Model.*, **36**(1), 139-157.

Gibson, K. and Ronald, F. (1994), *Principles of Composite Material Mechanics*, McGraw Hill, New York.

Goncalves, P.B. and Batista, R.C. (1987), "Frequency response of cylindrical shells partially submerged or filled with liquid", *J. Sound Vibr.*, **113**(1), 59-70.

Heidarzadeh, A., Kolahchi, R. and Rabani, B.M. (2016), "Concrete pipes reinforced with AL2O3 nanoparticles considering agglomeration: Magneto-thermo-mechanical stress analysis", *J. Civil Eng.*, 1-8.

Jain, R.K. (1974), "Vibration of fluid-filled orthotropic cylindrical shells", *J. Sound Vibr.*, **37**(3), 379-388.

Junger, M.C. and Mass, C. (1952), "Vibration of elastic shells in a fluid medium and the associated radiation of sound", *J. Appl. Mech.*, **74**, 439-445.

Kadoli, R. and Ganesan, N. (2003), "Free vibration and buckling analysis of composite cylindrical shells conveying hot fluid", *Compos. Struct.*, **60**(1), 19-32.

Matsuna, H. (2007), "Vibration and buckling of cross-ply laminated composite circular cylindrical shells according to a global higher-order theory", *J. Mech. Sci.*, **49**(9), 1060-1075.

Messina, A. and Soldatos, K.P. (1999), "Vibration of completely free composite plates and cylindrical shell panels by a higher-order theory", *J. Mech. Sci.*, **41**(8), 891-918.

Nguyen-Van, H., Mai-Duy, N., Karunasena, W. and Tran-Cong, T. (2011), "Buckling and vibration analysis of laminated composite plate/shell structures via a smoothed quadrilateral flat shell element with in-plane rotations", *Compos. Struct.*, **89**(7), 612-625.

Pellicano, F. and Amabili, M. (2003), "Stability and vibration of empty and fluid-filled circular cylindrical shells under static and periodic axial loads", *J. Sol. Struct.*, **40**(13), 3229-3251.

Rahmani, O., Khalili, S.M.R. and Malekzadeh, K. (2010), "Free vibration response of composite sandwich cylindrical shell with flexible core", *Compos. Struct.*, **92**(5), 1269-1281.

Ray, M.C. and Reddy, J.N. (2005), "Active control of laminated cylindrical shells using piezoelectric fiber reinforced composites", *Compos. Sci. Technol.*, **65**(7), 1226-1236.

Reddy, J.N. (2004), *Mechanics of Laminated Composite Plates and Shells-Theory and Analysis*, CRC Press, New York, U.S.A.

Safari, B.B., Kolahchi, R. and Rabani, B.M. (2016), "Buckling of

concrete columns retrofitted with nano-fiber reinforced polymer (NFRP)", *Comput. Concrete*, **18**(5), 1053-1063.
Tan, H., Huang, Y., Liu, C. and Geubelle, P.H. (2005), "The mori-tanaka method for composite materials with nonlinear interface debonding", *J. Plast.*, **21**(10), 1890-1918.
Tan, P. and Tong, L. (2001), "Micro-electromechanics models for piezoelectric-fiber-reinforced composite materials", *Compos. Sci. Technol.*, **61**(5), 759-769.
Tj, H.G., Mikami, T., Kanie, S. and Sato, M. (2005), "Free vibrations of fluid-filled cylindrical shells on elastic foundations", *Thin-Wall. Struct.*, **43**(11), 1746-1762.
Zamanian, M., Kolahchi, R. and Rabani, B.M. (2016), "Agglomeration effects on the buckling behaviour of embedded concrete columns reinforced with SiO2 nano-particles", *Wind Struct.*, **24**(1), 43-57.
Zhang, C., Zhou, W., Ma, G., Hu, C. and Li, S. (2015), "A meso-scale approach to modeling thermal cracking of concrete induced by water-cooling pipes", *Comput. Concrete*, **15**(4), 485-501.
Zhu, Z., Qiang, S. and Chen, W. (2013), "A new method solving the temperature field of concrete around cooling pipes", *Comput. Concrete*, **11**(5), 441-462.

CC